Contact Stress Distribution and Leakage Risk Control of Rotary Shaft Lip Seals

Jing Wang[1,*], Zhonghua Zhou[2]

[1] Chongqing Technology and Business Institute, Chongqing Open University, Chongqing 401520, China

[2] China Oilfield Services Limited, Sanhe 065200, Hebei, China

Corresponding Author: Jing Wang (1065560315@qq.com)

Funding: Scientific and Technological Research Project of Chongqing Municipal Education Commission (No. KJQN202204018): Research on Sealing Mechanism of Mechanical Equipment Lip Seal

Abstract: Rotary shaft lip seal in high-speed transmission, pump shaft and vehicle power system to assume the function of media retention and pollution isolation, lip contact stress attenuation will induce oil film rupture and leakage channel expansion. In order to improve the recognition accuracy of seal state, this paper established a finite element contact model between lip and rotating shaft, introduced parameters such as interference, spring preload, friction coefficient, speed load and interface temperature rise, and used local mesh encryption and surface-surface contact algorithm to solve the stress distribution. At the same time, the stress cloud map is transformed into the average contact stress, the proportion of low-pressure area, the continuity of contact zone and the circumferential fluctuation coefficient. Combined with the temperature rise and wear depth, the leakage risk identification and structural optimization method are constructed, and the engineering control process that can be calculated, judged and feedback is formed. The results show that the peak values of contact stress at 1000, 3000 and 5000 r/min are about 0.46, 0.39 and 0.31 MPa, respectively. After 90 minutes of operation, the risk index of the optimized structure is 0.43, which is 34.8% lower than that of the conventional structure. The research can provide a basis for lip seal design, condition evaluation and active leakage control.

Keywords: Rotary shaft lip seal; Contact stress distribution; Leakage risk control; Finite element simulation

1. Introduction

Rotary shaft lip seal is widely used in reducer, pump shaft, motor bearing, vehicle transmission system and aviation power plant, and its performance directly affects the maintenance of lubricating medium, isolation of external pollutants and operation reliability of rotating parts [1]. The coupling between lip and shaft surface is in the state of small contact width, high-speed friction and temperature rise for a long time. Once the contact stress distribution appears local attenuation or circumferential uneven, it is easy to induce oil film rupture, lip wear aggravation and leakage channel formation [2-3]. Previous studies have analyzed the lip seal failure from the perspective of material wear, thermo-structure coupling, axial surface roughness, eccentric assembly and mixed lubrication.

Finite element simulation has also been used to calculate the lip contact pressure and temperature field changes. In recent years, studies have further focused on the influence of high-speed working conditions, shaft eccentricity and surface processing methods on leakage performance [3-5]. The relevant results provide a basis for the mechanism analysis of the sealing interface. However, there are still some problems in the engineering application, such as insufficient connection between the contact stress cloud map and the leakage risk index, difficulty in directly transforming the simulation results into control parameters, and lack of unified calculation process for risk judgment under different speed loads [6].

Based on this, this paper studies the contact stress distribution and leakage risk control of the rotary shaft lip seal. By establishing the finite element contact model of lip and shaft surface, the contact stress distribution characteristics under different operating conditions are obtained by introducing engineering parameters such as material nonlinearity, shaft surface roughness, rotational speed load and temperature rising wear. On this basis, a leakage risk identification method is constructed by fusing stress cloud features, contact width changes and operating parameters, and the seal stability is improved by optimizing lip structure parameters and risk threshold control. The focus of this paper is to combine simulation calculation, feature extraction and engineering test verification to clarify the corresponding relationship between local lip stress attenuation and increased leakage risk. The research can provide technical reference for the design of rotating shaft lip seal structure, the evaluation of operating state and the active control of leakage risk.

2. Contact Failure Mechanism and Engineering Constraints of Rotary Shaft Lip Seal

2.1 Lip Contact Pressure Attenuation and Sealing Interface Leakage Formation Mechanism

The effective sealing of the rotary shaft lip seal depends on the continuous barrier formed by the lip preload and the contact pressure of the shaft surface. In the process of operation, the high-speed slip of the axial surface will cause the friction temperature to rise, and the rubber material will undergo thermal softening and compression permanent deformation, and the lip contact width and peak pressure will decrease. When the local contact pressure is lower than the oil film back pressure or the medium pulsating pressure, the sealing interface will have a micro-gap, and the lubrication medium will expand along the axial rough peak and valley and wear trench, gradually forming a leakage channel [7]. The contact pressure attenuation can be expressed as follows:

$$P_t = P_0 \cdot e^{-\alpha T - \beta W - \gamma n} \tag{1}$$

Where, P_t is the lip contact pressure after operation, P_0 is the initial contact pressure, T is the interface temperature rise, W is the amount of wear, n is the shaft speed, α, β, γ represent the influence coefficient of temperature rise, wear and speed on pressure attenuation respectively. The relationship can reflect the engineering law of heat-wear-rotational coupling of lower lip sealing capability decline.

2.2 Sealing Performance Degradation Characteristics Under the Coupling Condition of Speed Temperature Rise and Wear

The rotary shaft lip seal is affected by centrifugal disturbance, friction heating and material wear in high-speed operation. The increase of the rotational speed will increase the relative slip speed between the lip and the axial surface, and the thickness of the interface oil film and the friction heat will change synchronously. After the temperature rise continues to accumulate, the elastic recovery ability of the rubber lip decreases, and the preload weakens. The wear groove further destroys the

continuity of the contact zone and gradually penetrates the local microchannel [8]. The degree of seal degradation can be expressed by the comprehensive performance attenuation coefficient:

$$D_s = \lambda_1 \frac{v_r}{v_0} + \lambda_2 \frac{\Delta\theta}{\theta_0} + \lambda_3 \frac{h_m}{h_0} \quad (2)$$

Where, D_s is the attenuation coefficient of sealing performance, v_r is the linear velocity of axis surface, $\Delta\theta$ is the temperature rise of interface, hm is the wear depth of lip, v_0, θ_0 and h_0 are the corresponding reference values, λ_1, λ_2 and λ_3 are the weight coefficients. Table 1 lists the impact paths of different engineering factors on seal degradation.

Table 1: Sealing Performance Degradation Characteristics Under the Coupling of Speed Temperature Rise and Wear.

Engineering Factor	Main Change	Degradation Manifestation	Leakage Risk Impact
Increased rotational speed	Higher sliding velocity	Enhanced oil film fluctuation in the contact band	Medium-high risk
Temperature accumulation	Intensified thermal softening of rubber	Reduced lip preload force	High risk
Increased wear	Expansion of grooves on the contact surface	Discontinuity of the local sealing band	High risk
Eccentric vibration	Uneven circumferential pressure distribution	Periodic enlargement of local gaps	Medium-high risk

3.1 Calculation Method of lip Contact Stress Distribution Based on Finite Element Simulation

3.1.1 Geometric Modeling and Meshing of Lip Contact Area

In the lip-mouth contact area modeling, a two-dimensional axisymmetric finite element model is established with the core geometric parameters of the radius of the rotation axis, the interference of the lip, the Angle between the main and auxiliary lips, and the spring pretension position. The transition fillet of the lip tip, the micro-rough layer of the shaft surface, and the compression deformation area of the lip are separately divided into local fine regions [9]. In order to enhance the expression of the model to the engineering assembly state, the lip aperture contour is described in a parametric way:

$$\rho_l(s) = r_a - \delta_i + s \sin \varphi_l \quad (3)$$

Where $\rho_l(s)$ is the radial position of the lip contour point, r_a is the radius of the rotation axis, δ_i is the initial interference, s is the arc length coordinate of the lip contour, φ_l is the lip contact Angle. This equation can directly transform the assembly compression into the initial state of contact.

When meshes, an adaptive encryption strategy is used for lip tip contact zone, fillet transition zone and near surface layer of axial surface. The element size is adjusted according to curvature and pre-contact stress gradient:

$$l_e = \frac{l_{max}}{1 + \frac{\kappa_c}{\kappa_b} + \frac{|\nabla \sigma_p|}{\sigma_b}} \quad (4)$$

Where le is the local element size, l_{max} is the maximum element size, κ_c is the contact boundary curvature, κb is the fiduciary curvature, $\nabla\sigma_p$ is the pre-contact stress gradient, and σ_b is the fiduciary stress. Through this grid control method, the precision of stress calculation of lip small contact band can be improved.

3.1.2 Contact Stress Solution Under Speed Load Boundary Conditions

In the solution of contact stress, the shaft speed, spring preload, lip interference assembly and interface temperature rise are input into the finite element model as the main boundary conditions. The rotation axis is set as a rigid rotation boundary, the outer circle of the seal skeleton imposes a fixed constraint, the surface-surface contact algorithm is used between the lip and the shaft surface, and the friction contact and thermal expansion correction are introduced, so that the model can reflect the real engineering working conditions under high-speed slip [10]. The contact solution governing equation is as follows:

$$K_c u_r = F_i + F_s + F_\omega + F_\theta \tag{5}$$

Where, K_c is the contact stiffness matrix, u_r is the joint displacement vector, F_i is the interference assembly load, F_s is the spring preload, Fω is the rotational speed induced load, and F_θ is the temperature rise deformation load.

The contact stress of lip joints is calculated according to local normal load and effective contact area:

$$\sigma_{c,j} = \frac{N_j + \mu Q_j}{A_j} \tag{6}$$

Where $\sigma_{c,j}$ is the equivalent contact stress of the JTH contact node, N_j is the normal contact load, Q_j is the tangential friction load, μ is the friction coefficient, and A_j is the effective contact area corresponding to the node. In order to ensure the engineering reproducibility of the simulation results, the main parameter Settings of the model are shown in Table 2.

Table 2: Main Parameter Settings of the FE Simulation Model.

Parameter Category	Parameter Name	Setting Range	Engineering Function
Geometric parameter	Rotary shaft diameter	35 mm	Determines the sealing contact radius
Geometric parameter	Lip interference	0.12–0.22 mm	Affects the initial contact pressure
Material parameter	Rubber elastic modulus	6–12 MPa	Reflects the rebound capability of the lip
Material parameter	Poisson's ratio	0.49	Characterizes the nearly incompressible behavior of rubber
Contact parameter	Friction coefficient	0.08–0.18	Controls the interfacial shear stress
Operating parameter	Shaft rotational speed	1000–5000 r/min	Simulates different high-speed operating conditions
Thermal boundary parameter	Interface temperature	25–90 ℃	Represents the effect of frictional temperature rise

By setting the boundary conditions above, assembly, rotational speed, friction and temperature rise can be incorporated into the contact stress solution process, which provides reliable simulation input for subsequent leakage risk identification.

3.2 Leakage Risk Identification Method by Fusing Stress Cloud Map and Operating Parameters

After solving the contact stress, this paper converts the lip stress cloud map output by the finite element into computable features, and fuses them with the operating parameters such as speed, temperature rise, and wear depth. The specific approach is to perform gray mapping and region segmentation on the contact zone nodes, and extract the peak contact stress, the proportion of low-pressure area, the continuity of the contact zone and the circumferential stress fluctuation coefficient, so as to avoid judging the sealing state only by the maximum value of a single point [11]. The proportion of low-pressure area can be expressed as follows:

$$R_l = \frac{A_l}{A_c} \tag{7}$$

Where, R_l is the proportion of the low-pressure area, A_l is the area of the contact stress below the threshold, and Ac is the effective contact area of the lip. When the low-pressure zone is continuously extended along the axial or circumferential direction, the leakage risk will increase significantly.

The comprehensive leakage risk index can be expressed as follows:

$$L_r = \eta_1 \left(1 - \frac{\bar{\sigma}_c}{\sigma_0}\right) + \eta_2 R_l + \eta_3 \frac{\Delta\theta}{\theta_0} + \eta_4 \frac{h_m}{h_0} \tag{8}$$

Where, L_r is the leakage risk index, $\bar{\sigma}_c$ is the average contact stress, σ_0 is the design reference contact stress, $\Delta\theta$ is the interface temperature rise, hm is the wear depth, η_1, η_2, η_3, η_4 are the index weights. This method can unify the simulation cloud image, sensor monitoring and wear measurement results into the same risk judgment framework.

Table 3: Leakage Risk Identification Index and Determination Threshold.

Identification Indicator	Data Source	Low-Risk Threshold	Medium-Risk Threshold	High-Risk Threshold
Average contact stress	Finite element stress cloud map	≥0.42 MPa	0.30–0.42 MPa	<0.30 MPa
Low-pressure area ratio	Cloud map region segmentation	<15%	15%–30%	>30%
Contact band continuity	Contact node connectivity calculation	Continuity rate ≥92%	80%–92%	<80%
Circumferential stress fluctuation coefficient	Node stress statistics	<0.18	0.18–0.32	>0.32
Interface temperature rise	Temperature sensor	<25 ℃	25–45 ℃	>45 ℃
Lip wear depth	Profile measurement	<0.04 mm	0.04–0.08 mm	>0.08 mm

Through the combination of the above indicators, the leakage risk no longer stays at the empirical judgment level, but is transformed into a recognition result that can be calculated, thresholder, and used for engineering early warning.

3.3 Lip Structure Parameter Optimization and Risk Control Method for Seal Stability

For leakage risk control, lip Angle, interference, spring preload and contact belt width are used as adjustable structural parameters, which are coordinately optimized according to contact stress uniformity and the proportion of low pressure area. In the optimization process, the finite element model first outputs the stress distribution results under different parameter combinations, and then feeds back the risk index to the structural parameter correction module to keep the lip contact pressure in a stable interval [12-13]. The structure optimization objective can be expressed as follows:

$$J = \min\left[\omega_1 C_\sigma + \omega_2 R_l + \omega_3 \left|\frac{b_c - b_0}{b_0}\right|\right] \tag{9}$$

Where, J is the comprehensive optimization objective, C_σ is the contact stress fluctuation coefficient, R_l is the proportion of low-pressure area, b_c is the actual contact band width, b_0 is the designed contact band width, ω_1, ω_2, ω_3 are the weight coefficients. This method can ensure the continuity of lip contact and reduce the risk of leakage caused by the expansion of local low-pressure area. Figure 1 shows the schematic of lip structure parameter optimization and risk control path.

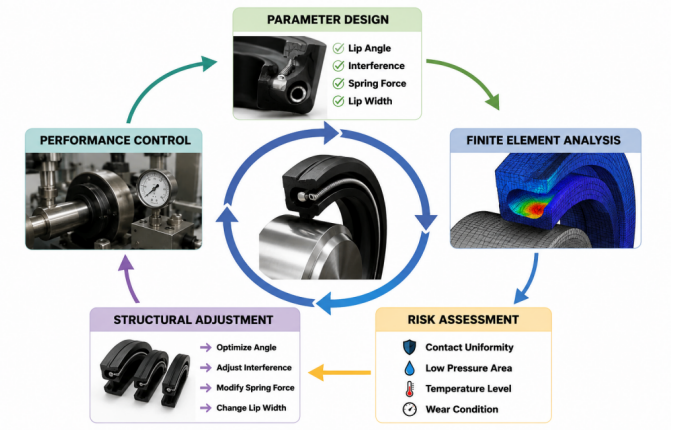

Figure 1: Schematic Diagram of lip Structure Parameter Optimization and Risk Control Path.

4. Test Analysis of Sealing Contact Stress and Leakage Risk

In order to verify the engineering applicability of the contact stress distribution calculation and leakage risk control method of rotating shaft lip seal, this paper established a rotating shaft sealing performance test platform. The test object is NBR lip seal with 45 steel rotating shaft. The surface roughness of the shaft is controlled within the range of Ra 0.2-0.4μm. Standard lubricating oil is added into the sealing chamber as the medium. The test platform is composed of variable frequency drive motor, torque speed sensor, temperature acquisition module, pressure loading device, micro leakage collection unit and data acquisition system. The speed range is set to 1000-5000 r/min, the pressure of the sealing chamber is controlled at 0.05-0.20 MPa, and the ambient temperature is maintained at about 25℃ [14]. In the finite element simulation part, the geometric model of lip and rotation axis was established by SolidWorks, and imported into ANSYS to solve the contact stress.

The speed, temperature rise, friction torque and leakage of the test data were recorded in real time through the LabVIEW acquisition interface [15]. Each group of working conditions was run continuously for 30 min, and the data of the stable phase were taken for analysis and compared with the simulation results. Through this test environment, the effects of speed load, friction temperature rise and lip wear on contact stress attenuation and leakage risk change can be investigated simultaneously.

4.1 Lower Lip Contact Stress Distribution Test Under Different Rotational Speed Loading Conditions

In order to verify the reliability of the finite element contact stress calculation results, three sets of speed conditions of 1000 r/min, 3000 r/min and 5000 r/min are set in this paper, and the sealing chamber pressure of 0.05 MPa, 0.10 MPa and 0.20 MPa is superimposed respectively. The equivalent contact stress at different width positions of the lip-mouth contact belt was collected [16]. In the test, the film pressure sensor was checked with the simulation node results, and the contact width direction was taken as the analysis interval of 0-0.60mm. Figure 2 shows the distribution curves of the contact stress along the lip width under different speed loads.

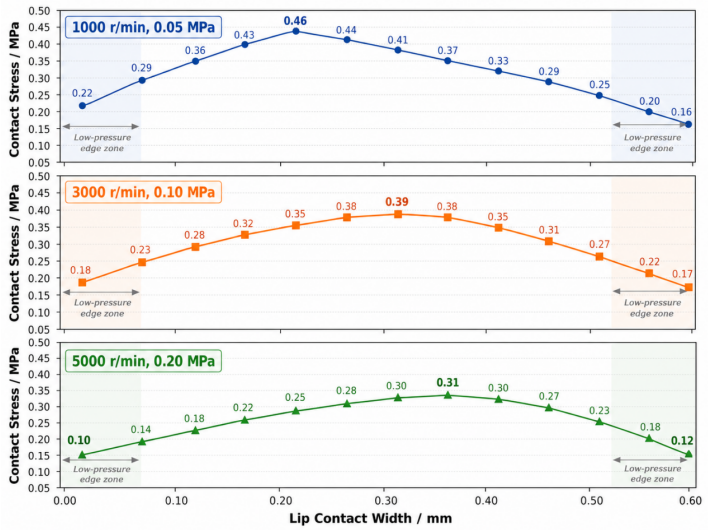

Figure 2: Distribution Curves of Contact Stress Along Lip Width Under Different Speed Loads.

The results show that the peak stress is about 0.46 MPa at low speed, and the curve distribution is gentle. When the rotation speed increased to 3000 r/min, the peak stress decreased to 0.39 MPa, and the peak position shifted to the outside. The peak value is further reduced to 0.31 MPa under high speed and high-pressure conditions, and the low-pressure area at the edge of the contact zone is significantly expanded. It shows that when the speed load increases, the friction temperature rise and lip deformation will weaken the continuity of contact pressure, and the leakage risk will increase.

4.2 Leakage Risk Control Effect Test Under Coupling of Temperature Rise and Wear

In order to verify the risk control effect of optimized lip structure parameters, this paper sets up two groups of comparative tests of conventional seal structure and optimized seal structure, which run continuously for 90 min at 3000 r/min speed and 0.15 MPa seal chamber pressure, and simultaneously collect interface temperature rise, lip wear depth, trace leakage and leakage risk index

[17]. Figure 3 shows the change curve of the leakage risk index under the coupling of temperature rise and wear.

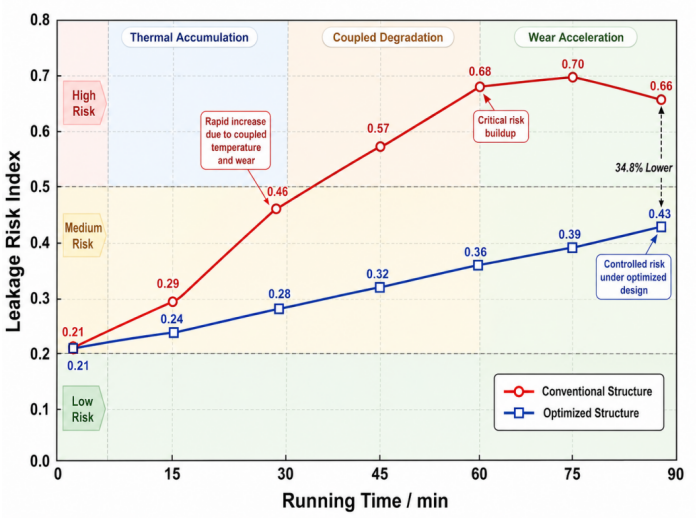

Figure 3: Change Curve of Leakage Risk Index Under Coupling of Temperature Rise and Wear

21 to 0.46 after 30 minutes of operation, and reaches 0.68 after 60 minutes. The leakage risk increases significantly due to the influence of temperature rise accumulation and wear groove expansion in the later period. The optimized structure keeps the width of the contact belt stable by adjusting the lip Angle, interference amount and spring preload. The risk index is controlled at 0.43 at 90 min, which is about 34.8% lower than that of the conventional structure. It shows that the parameter optimization can suppress the expansion of low pressure area and the amplification effect of lip wear, and improve the stability of the seal.

5. Conclusion

Focusing on the contact stress distribution and leakage risk control of rotary shaft lip seal, the finite element simulation, cloud image feature extraction and risk threshold determination methods are constructed in this paper. Through parametric modeling, local mesh encryption, rotational speed loading and friction thermal correction, the effects of lip interference, spring pretension, shaft surface slip and temperature rise wear on the contact pressure are described. The test shows that the peak value of contact stress decreases from 0.46MPa to 0.31MPa with the increase of speed and pressure of the sealing chamber, and the low-pressure area of the edge expands, and the leakage risk increases. After the optimization of lip Angle, interference and spring preload, the risk index was controlled at 0.43 in 90 min operation stage, which was 34.8% lower than that of the conventional structure, indicating that the method can inhibit the expansion of low-pressure area and the penetration of wear grooves. Subsequently, online sensing and digital twin model can be combined to realize real-time prediction of seal state and life maintenance.

References

[1] Fazekas B, Burkhart C, Staub S, Thielen S, Andrä H, Goda T J, Sauer B, Koch O. Radial shaft seals: How ageing in oil and hyper-viscoelasticity affect the radial force and the numerically predicted wear. Tribology International, 2023, 186: 108601. DOI: 10.1016/j.triboint.2023.108601.

[2] Morad O, Saikko V, Viitala R. Performance characterization of marine lip seals: Contact temperature and frictional torque. Wear, 2023, 523: 204763. DOI: 10.1016/j.wear.2023.204763.

[3] Morad O, Viitala R, Saikko V. Behavior of marine thruster lip seals under typical operating conditions. Tribology International, 2025, 201: 110195. DOI: 10.1016/j.triboint.2024.110195.

[4] Nomikos P, Rahmani R, Morris N, Rahnejat H. An investigation of oil leakage from automotive driveshaft radial lip seals. Proceedings of the Institution of Mechanical Engineers, Part D: Journal of Automobile Engineering, 2023, 237(13): 3108-3124. DOI: 10.1177/09544070221127105.

[5] Nomikos P, Rahmani R, Morris N, Rahnejat H. Measurement and prediction of thermal performance of automotive transmission radial lip seals. Proceedings of the Institution of Mechanical Engineers, Part D: Journal of Automobile Engineering, 2023: 1-17. DOI: 10.1177/09544070231213903.

[6] Grün J, Gohs M, Bauer F. Multiscale structural mechanics of rotary shaft seals: Numerical studies and visual experiments. Lubricants, 2023, 11(6): 234. DOI: 10.3390/lubricants11060234.

[7] Hahn S, Feldmeth S, Bauer F. Assessment of the lubricity of grease-sealing rotary shaft seals based on grease properties. Chemical Engineering & Technology, 2023, 46(1): 53-60. DOI: 10.1002/ceat.202200382.

[8] Fricker P, Baumann M, Bauer F. How wetting properties influence the wear of radial lip sealing systems. Chemical Engineering & Technology, 2023, 46(1): 61-70. DOI: 10.1002/ceat.202200375.

[9] Hannss J, Grün J, Olbrich C, Feldmeth S, Bauer F. Multiphase conjugate heat transfer analyses on the assembly situation of rotary shaft seals. Applied Sciences, 2023, 13(19): 11026. DOI: 10.3390/app131911026.

[10] Engelfried M, Haffner G, Baumann M, Bauer F. Modeling the pumping behavior of macroscopic lead structures on shaft counterfaces of rotary shaft seals. Lubricants, 2023, 11(11): 495. DOI: 10.3390/lubricants11110495.

[11] Thielen S, Subramanian T, Sauer B, Koch O, Börner R, Junge T, Schubert A. Characterisation of the conveying effect of turned radial shaft seal counter-surfaces using a simplified hydrodynamic simulation model. Forschung im Ingenieurwesen, 2023, 87: 655-671. DOI: 10.1007/s10010-023-00610-9.

[12] Stiemcke Y, Thielen S, Koch O, Schollmayer T, Sauer B. Investigation of the effect of underpressure between main and dust lip on the performance of radial shaft seals under instationary shaft movements. Journal of Tribology, 2024, 146(6): 064401. DOI: 10.1115/1.4064511.

[13] Stubbe L, Stiemcke Y, Mross S, Staub S, Steiner K, Münnemann K, Koch O, Thielen S. A new rubber-lubricant compatibility test on a tribometer for radial shaft seals. Tribologie und Schmierungstechnik, 2025, 71(5-6): 38-44. DOI: 10.24053/TuS-2024-0037.

[14] Stiemcke Y, Thielen S, Koch O. Theoretical concept for in-situ condition monitoring of rotary shaft seals using surface strain-based analysis of the deformation state. Forschung im Ingenieurwesen, 2025, 89(1): 61. DOI: 10.1007/s10010-025-00819-w.

[15] Stiemcke Y, Rheinländer C, Feldmann J, Uebel J, Becker T, Nikolaus K, Seewig J, Wehn N, Koch O, Sauer B, Thielen S. Integrated sensor system for rotary shaft seals enabling condition monitoring of dynamic sealing contact and lubricant. Forschung im Ingenieurwesen, 2025, 89: 116. DOI: 10.1007/s10010-025-00888-x.

[16] Schollmayer T, Thielen S, Schröder V, Sauer B, Koch O. Experimental investigation of radial shaft seal followability against dynamic shaft displacement without shaft rotation at low temperatures. Journal of Tribology, 2025, 147(10): 104401. DOI: 10.1115/1.4069086.

[17] Szczęch M. Research into the pressure capability and friction torque of a rotary lip seal lubricated by ferrofluid. Journal of Magnetism and Magnetic Materials, 2025, 614: 172759. DOI: 10.1016/j.jmmm.2024.172759.